Mathematics

http://www.aimspress.com/journal/Math

AIMS Mathematics, 9(1): 2500–2517.
DOI: 10.3934/math.2024123
Received: 08 October 2023
Revised: 26 November 2023
Accepted: 08 December 2023
Published: 25 December 2023

Research article

Response of vegetation pattern to climate change based on dynamical model: Case of Qinghai Lake, China

Juan Liang[1,2,*], **Huilian Ma**[1], **Huanqing Yang**[1] **and Zunguang Guo**[1,*]

[1] Department of Science, Taiyuan Institute of Technology, Taiyuan 030008, China
[2] Department of Mathematics, North University of China, Taiyuan 030051, China

* **Correspondence:** Email: liangjuan76@126.com, guozg@tit.edu.cn.

Abstract: The global climate has undergone great changes in recent decades, which has a significant impact on the vegetation system, especially in arid and semi-arid areas. Based on a dynamic model, this paper studied the response of vegetation pattern to climate change in Qinghai Lake, a typical semi-arid region. The conditions for Turing instability of the equilibrium were obtained by mathematical analysis. The numerical experiments showed the influence of different climitic factors (carbon dioxide concentrations $[CO_2]$, temperature and precipitation) on vegetation pattern. The results showed that the robustness of the vegetation system was enhanced as precipitation or $[CO_2]$ increased. Furthermore, we presented evolution of vegetation system under different climate scenarios to forecast the future growth of vegetation. We compared the various climate scenarios with representative concentration pathways (RCP2.6, RCP4.5, RCP8.5). The results revealed that RCP2.6 scenario was a desired climate scenario for Qinghai Lake. Our study also highlighted the measures to avoid desertification by the method of optimal control. We expect that this study will provide theoretical basis for vegetation protection.

Keywords: climate change; vegetation pattern; optimal control; stability; Qinghai Lake
Mathematics Subject Classification: 34C23, 34K20, 49J20

1. Introduction

Modern climate change is a world problem that is paid general attention to by all of mankind. Global climatic variability not only affects the living environment of human beings, but also affects the world economic development and social progress. Over the past 100 years, the global climate has been facing a dramatic change distinguished by temperature increasing [1–4], which was related to both natural factors and human activities. The global surface temperature between 2011 and 2020 was 1.1(°C) greater than that between 1850 and 1900. From 1975 to 2014, CO_2 concentrations $[CO_2]$ increased from 280 ppm to 387ppm [5]. Observational data from China indicates that the increase rate of the annual average temperature in China was much faster than the world during the last 50 years, especially the Tibetan Plateau [6, 7].

The Qinghai-Tibetan Plateau (QTP) has become one of the most typical areas affected by climate change [8]. That is because the QTP is the highest altitude region in the middle latitudes of the world, and the high latitudes and high elevations are more susceptible to global warming. In recent decades, the QTP has undergone rapid warming, and the warming rate is almost twice that of the world [9]. The precipitation has increased over the decades, which contributes to the rising of water levels and lakes expanding [10]. The climate change of the QTP has a great impact on the adjacent areas and serves as an indicator of global climate change [11]. The researches on climate change in the (QTP) have achieved abundant results [12–15].

Qinghai Lake, which is the biggest salt lake in China, is located in the northeast edge of the QTP at an altitude of about 3,200m, with longitude from 99°36′E to 100°47′E and latitude from 36°32′N to 37°15′N [16], as shown in Figure 1. Qinghai Lake is a natural barrier for controlling the eastward spread of desertification in the western region, while it lies in a monsoon transitional zone, and it is a famous tourism resort in China [17]. The average depth of the lake is 21 meters and the maximum depth exceeds 29 meters [18]. In the past 50 years, the average temperature in Qinghai Lake area increased by 0.319(°C) every 10 years [19]. It is a typical semi-arid region, Its heterogeneous environments are vulnerable to global climate variability and the ecosystem is fragile [20].

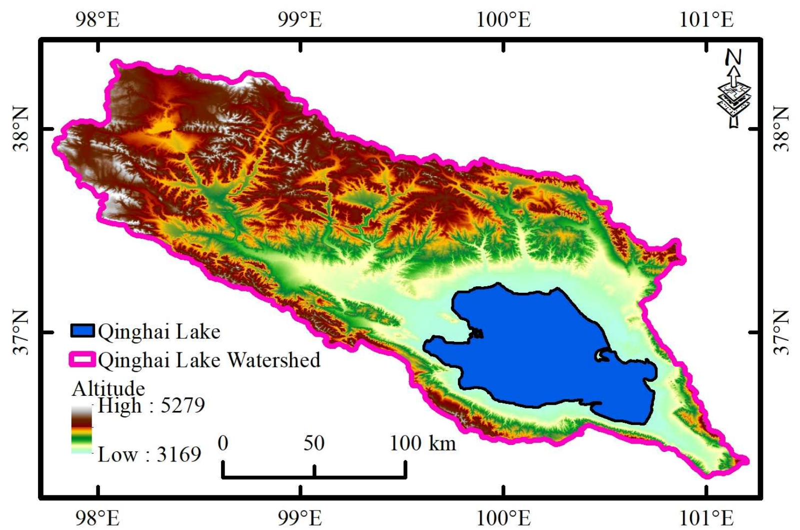

Figure 1. The location of Qinghai Lake.

In recent decades, Qinghai Lake has attracted increased attention [21–26]. Additionally, there have been some studies on the vegetation of Qinghai Lake. Zhang et al. studied vegetation change in the Qinghai Lake watershed by conducting pollen-based vegetation reconstruction at an archaeological site [27]. Wang et al. studied the relationship between grassland vegetation and climatic parameters in Qinghai Lake. The result showed that the main reason for the improvement of vegetation cover in the Qinghai Lake basin was the increase of precipitation [28]. The plant community characteristics of different sand-forming communities in the largest desert area on the East Coast of Qinghai Lake were studied and the results showed that species diversity of plant community and herb coverage were positively correlated with dune stability [29]. Cai et al. studied the effects of human activities and climate change on vegetation in Qinghai Lake basin [30]. We can see that most of the current researches on vegetation of the Qinghai Lake are based on observation data and statistical methods, paying little attention to spatial distribution and the growth of vegetation based on pattern dynamics. The evolution law of vegetation pattern can be qualitatively analyzed based on dynamic equation [31–35]. Therefore, in this paper, we present a reaction-diffusion equation and apply the pattern dynamics theory to reveal characteristics of temporal and spatial distribution of vegetation.

The study aims to address the question as follows: (1) How to establish a suitable vegetation-cilimitic dynamics model? (2) How do different climitic factors affect the growth of vegetation? (3) How will the vegetation pattern transform under different climate scenarios? (4) What are the measures to prevent desertification? In this study, the conditions of steady-state bifurcation are obtained via theoretical analysis. Moreover optimal control theory provides a framework for avoiding desertification of the ecosystem. Finally, we employ numerical simulations to verify the response of the vegetation system to climate change that aim to try to avoid desertification and enhance the robustness of the ecosystem.

2. The model

2.1. Model derivation

Water is an essential condition for maintaining the normal physiological function of vegetation. Water resource for vegetation growth mainly comes from precipitation. When rain falls to the ground, some water seeps into the soil and is absorbed by vegetation, then some forms surface runoff. Taken together, Klausmeier established a vegetation-water model in 1999 [36]:

$$\begin{cases} \frac{\partial N}{\partial t} = RJWN^2 - MN + D_N \Delta N, \\ \frac{\partial W}{\partial t} = A - LW - RWN^2 + V \frac{\partial W}{\partial X}, \end{cases} \tag{2.1}$$

where N and W represent the biomass of vegetation and water, respectively. A is the precipitation, the evaporation rate of water is L, vegetation takes up water at rate RWN^2, J is the rate of conversion of biomass per unit of water consumption, the natural mortality rate of vegetation is M, D_N is the diffusion coefficient of vegetation and water flows downhill at speed V.

It is worth mentioning that the shading effect of vegetation can reduce the evaporation rate of water. Here, we mainly consider the growth of vegetation on flat ground. At the same time, the carbon gain generated by photosynthesis promotes plant growth and the carbon loss generated by respiration consumes vegetation biomass. Most of the water absorbed by vegetation is lost to the atmosphere in the form of water vapor through transpiration. The major factors affecting these three physiological processes are $[CO_2]$ and temperature. Therefore, based on model (2.1) and the above facts, the dynamic model of vegetation and water is established as follows:

$$\begin{cases} \frac{\partial N}{\partial t} = C_g - R_{esp} N + D_N \Delta N, \\ \frac{\partial W}{\partial t} = A - (1 - \rho N) W - E_r + D_W \Delta W, \end{cases} \tag{2.2}$$

where ρ is the reduced evaporation rate of vegetation due to shading. D_W is the diffusion coefficient of water. The amount of vegetation growth C_g due to photosynthesis can be given by the following expression [37]:

$$C_g = C_a(1 - \frac{C_i}{C_a})C_1 R g_{co_2} W N^2,$$

where C_a is environmental CO_2 concentration, C_1 is the photosynthetic conversion coefficient of plant biomass and C_i is the available CO_2 concentration between canopy cells. The rate of vegetation loss due to respiration R_{esp} can be approximated by a Michaelis M_{10} function [37]:

$$R_{esp} = B_R M_{10}^{\frac{T-10}{10}},$$

where B_R describes the basic respiration per unit biomass.

E_r stands for transpiration of vegetation, which can describe the difference between saturation specific humidity, and actual specific humidity and the expression for E_r is as follows [37]:

$$E_r \approx g_{canopy}(q^* - q_a), \tag{2.3}$$

where g_{canopy} is for canopy water transfer, which is related to water absorbed by vegetation, and q is the dimensionless specific humidity. Based on the above analysis, let

$$g_{canopy} = g_{H_2O} RWN^2 = \gamma g_{CO_2} RWN^2,$$

where g_{H_2O} is the maximum conductivity to H_2O and CO_2, respectively and γ is the conversion coefficient of diffusivity difference between CO_2 and H_2O.

In (2.3), specific humidity is defined as follows: $q = \dfrac{\rho_v}{\rho_d}$, where $\rho_v(kgm^{-3})$ and $\rho_d(kgm^{-3})$ represent the density of water vapor and dry air, respectively. According to Dalton's law, there are

$$\rho_d = \frac{P - s}{R_d T_a}, \rho_v = \frac{0.622 s}{R_d T_a},$$

where P is atmospheric pressure, s is the pressure of steam, R_d is a constant and T_a is the absolute temperature. We assume that p is large enough and has $q^* = \frac{0.622 s^*}{P}$. According to the above analysis, E_r can be obtained:

$$E_r = R\gamma g_{co_2} WN^2 \frac{0.622}{P} s^*(1 - \frac{s}{s^*}).$$

According to the Clausius-Clapeyron function, the saturated vapor pressure is determined:

$$s^*(T) = 0.611 exp(\frac{17.502T}{T + 240.97}).$$

Let relative humidity be $R_h = \dfrac{s}{s^*}$ and one has

$$E_r = R\gamma g_{co_2} WN^2 \frac{0.622}{P} s^*(1 - R_h)).$$

Based on the above analysis, we obtained a bivariate dynamics model to study the vegetation growth in Qinghai Lake:

$$\begin{cases} \dfrac{\partial N}{\partial t} = JRg_{co_2} WN^2 - R_{esp} N + D_N \Delta N \quad \text{in} \quad U = \Omega \times (0, T), \\ \dfrac{\partial W}{\partial t} = A - (1 - \rho N)W - R\gamma g_{co_2} qWN^2 + D_W \Delta W \quad \text{in} \quad U, \end{cases} \tag{2.4}$$

with $J = C_a(1 - \frac{C_i}{C_a})C_1$ and $q = \frac{0.622}{P} e^*(1 - R_h))$. See appendix A for explanations of parameters in the model (2.4).

2.2. Stability analysis

In this subsection, we shall demonstrate the occurrence of the Turing pattern by stability analysis for system (2.4). The steady states of (2.4) are

$$E_0 = (0, A),$$
$$E_1 = (\frac{ARg_{co_2}J + R_{esp}\rho + \sqrt{\Phi}}{2\gamma qR_{esp}Rg_{co_2}}, \frac{ARJg_{co_2} + R_{esp}\rho - \sqrt{\Phi}}{2g_{co_2}RJL}),$$
$$E_2 = (\frac{ARg_{co_2}J + R_{esp}\rho - \sqrt{\Phi}}{2\gamma qR_{esp}Rg_{co_2}}, \frac{ARJg_{co_2} + R_{esp}\rho + \sqrt{\Phi}}{2g_{co_2}RJL}),$$

where $\Phi = (ARJg_{co_2} + \rho R_{esp})^2 - 4R\gamma g_{co_2}qR_{esp}^2$, E_1 and E_2 only exist if $\Phi > 0$. E_0 is the bare ground equilibrium.

In what follows, the stability of the steady states will be discussed. We assume the condition $\Phi > 0$ holds so that E_1 and E_2 are biologically meaningful.

Let

$$F(N, W) = JRg_{co_2}WN^2 - R_{esp}N, G(N, W) = A - LW - R\gamma qg_{co_2}WN^2.$$

The linearization of (2.4) at E^* is

$$\begin{pmatrix} \frac{\partial N}{\partial t} \\ \frac{\partial W}{\partial t} \end{pmatrix} = D\Delta \begin{pmatrix} N \\ W \end{pmatrix} + M \begin{pmatrix} N \\ W \end{pmatrix} \tag{2.5}$$

with

$$D\Delta = \begin{pmatrix} D_N\Delta & 0 \\ 0 & D_W\Delta \end{pmatrix}, M = \begin{pmatrix} a_{11} & a_{12} \\ a_{21} & a_{22} \end{pmatrix},$$

where

$$a_{11} = 2g_{co_2}JRN^*W^* - R_{esp}, \quad a_{12} = g_{co_2}JRN^{*2},$$
$$a_{21} = -2g_{co_2}\gamma qRN^*W^*, \quad a_{22} = -g_{co_2}\gamma qRN^{*2} - L.$$

Consider the spatially heterogeneous perturbations [38, 39]:

$$\begin{pmatrix} N \\ W \end{pmatrix} = \begin{pmatrix} N* \\ W* \end{pmatrix} + \begin{pmatrix} c_1 \\ c_2 \end{pmatrix} e^{\lambda t + i\kappa x} + c.c + O(\varepsilon^2),$$

where κ is a wave-number and λ reprsents a growth rate of perturbation in t. Substituting the above formula into (2.5), the characteristic equation is given:

$$detM = \begin{vmatrix} a_{11} - D_N\kappa^2 - \lambda & a_{12} \\ a_{21} & a_{22} - D_W\kappa^2 - \lambda \end{vmatrix} = 0. \tag{2.6}$$

It follows from (2.6) that the characteristic equation of (2.5) is:

$$\lambda^2 + \beta_1(\kappa)\lambda + \beta_2(\kappa) = 0,$$

where

$$\beta_1(\kappa) = a_{11} + a_{22} - (D_N + D_W)\kappa^2,$$
$$\beta_2(\kappa) = D_N D_W\kappa^4 - (a_{11}D_W + a_{22}D_N)\kappa^2 + a_{11}a_{22} - a_{12}a_{21}.$$

In accordance with the above derivation, our result reads as follows.

Theorem 2.1. *Suppose that $\Phi > 0$, then the bare-soli steady state E_0 is always stable and the positive steady state E_2 is unstable.*

Proof. The characteristic equation corresponding to the bare-soli steady state E_0 is

$$\lambda^2 + \beta_1(\kappa)\lambda + \beta_2(\kappa) = 0,$$

where

$$\beta_1(\kappa) = (D_N + D_W)\kappa^2 + R_{esp} + 1,$$
$$\beta_2(\kappa) = (D_N\kappa^2 + R_{esp})(D_W\kappa^2 + 1).$$

It is easy to see that $\beta_1(\kappa) > 0$ and $\beta_2(\kappa) > 0$ ($\kappa = 0, 1, 2...$). Therefore, E_0 is always stable. Analogously, the characteristic equation is as follows for E_2:

$$\lambda^2 + \beta_1(\kappa)\lambda + \beta_2(\kappa) = 0,$$

where

$$\beta_1(\kappa) = (D_N + D_W)\kappa^2 + \frac{A^2J^2Rg_{CO_2} - 2R_{esp}^3 q\gamma + AJR_{esp}\rho - AJ\sqrt{\Phi}}{2R_{esp}^2 q\gamma},$$

$$\begin{aligned}\beta_2(\kappa) =& D_N D_W \kappa^4 + \frac{(A^2J^2RD_N g_{CO_2} - 2R_{esp}^3 D_W q\gamma + AJR_{esp}D_N\rho - AJD_N\sqrt{\Phi})\kappa^2}{2R_{esp}^2 q\gamma}\\ &+ \frac{1}{2R_{esp}Rg_{CO_2}q\gamma}(\Phi - AJR_{esp}g_{CO_2}\sqrt{\Phi} - R_{esp}\rho\sqrt{\Phi}).\end{aligned}$$

It is easily seen that $\beta_2(\kappa) < 0$ when $\kappa = 0$, then the positive steady state E_2 is unstable. □

In what follows we shall analyze the dynamic behavior of E_1. First, the characteristic equation is given:

$$\lambda^2 + \beta_1(\kappa)\lambda + \beta_2(\kappa) = 0,$$

where

$$\beta_1(\kappa) = (D_N + D_W)\kappa^2 + \frac{A^2J^2Rg_{CO_2} - 2R_{esp}^3 q\gamma + AJR_{esp}\rho + AJ\sqrt{\Phi}}{2R_{esp}^2 q\gamma},$$

$$\begin{aligned}\beta_2(\kappa) =& D_N D_W \kappa^4 + \frac{(A^2J^2RD_N g_{CO_2} - 2R_{esp}^3 D_W q\gamma + AJR_{esp}D_N\rho + AJD_N\sqrt{\Phi})\kappa^2}{2R_{esp}^2 q\gamma}\\ &+ \frac{1}{2R_{esp}Rg_{CO_2}q\gamma}(\Phi + AJR_{esp}g_{CO_2}\sqrt{\Phi} + R_{esp}\rho\sqrt{\Phi}).\end{aligned}$$

It is easy to check that $\beta_2(0) > 0$ when $\kappa = 0$. Based on the above discussion, the result reads as follows.

Theorem 2.2. *Suppose that $\Phi > 0$ holds. If $D_N = D_W = 0$, then E_2 is stable for $\beta_1(0) > 0$ and unstable for $\beta_1(0) < 0$.*

On the basis of the Turing theory, we can conclude that system (2.4) induces Turing pattern under the two conditions: First, E_2 is stable without diffusion; Second, E_2 is unstable in the presence of diffusion. As a result, Turing instability occurs only provided that $\beta_1(0) > 0$ and $\beta_1(\kappa) < 0$ for some $\kappa \in \mathbb{N}^+$.

3. The optimal control problem

Based on the condition for Turing instability deduced in part two, the vegetation patterns with different structures can be presented by numerical experiments. With the increase of precipitation A, vegetation patterns change from spot structure to stripe structure (shown in Figure 2), which implies that the robustness of the ecological system is enhanced. Therefore, we can prevent the degradation of the vegetation ecosystem by controlling pattern formations. Here, we aim to get the stripe structure under the case of low precipitation. The optimal control problem provides a powerful tool to realize the aim. We regard the artificial planting rate $r(x,t)$ as a control parameter and rewrite system (2.4) as follows:

$$\begin{cases} \dfrac{\partial N}{\partial t} = JRg_{co_2}WN^2 - R_{esp}N + rN + D_N\Delta N \quad \text{in} \quad U, \\ \dfrac{\partial W}{\partial t} = A - (1-\rho N)W - R\gamma g_{co_2}qWN^2 + D_W\Delta W \quad \text{in} \quad U. \end{cases} \tag{3.1}$$

The set of admissible controls for $r(x,t)$ is [40]:

$$\Lambda_{ad} = \{r \in L^{\infty}(U) | r_1 < r(x,t) < r_2 \quad \text{a.e. in} \quad U\}.$$

The objective functional expresses a trade-off between the desired precision and a cost of achieving such precision. Specifically, optimal control aims to lower costs (artificial planting amount) while making the uncontrolled pattern $(N(x,T), W(x,T))$ approach the target pattern $(N_T(x), W_T(x))$. Consider the following optimal control problem:

$$\min_{r\in\Lambda_{ad}} J[N,W] = \frac{b_1}{2}\int_{\Omega}[N(x,T)-N_T(x)]^2dx+\frac{b_2}{2}\int_{\Omega}[W(x,T)-W_T(x)]^2dx+\frac{c}{2}\int_0^T\int_{\Omega} r^2(x,t)dxdt, \tag{3.2}$$

subject to

$$\begin{cases} \dfrac{\partial N}{\partial t} = D_N\Delta N + f_1(n,w,r) \quad \text{in} \quad U, \\ \dfrac{\partial W}{\partial t} = D_W\Delta W + f_2(n,w,r) \quad \text{in} \quad U, \\ \dfrac{\partial N}{\partial n} = 0, \dfrac{\partial W}{\partial n} = 0 \quad \text{on} \quad U = \partial\Omega \times (0,T), \\ N(x,0) = N_0(x), W(x,0) = W_0(x) \quad \text{in} \quad U, \end{cases} \tag{3.3}$$

where

$$f_1(n,w,r) = JRg_{co_2}WN^2 - R_{esp}N + r,$$

$$f_2(n,w,r) = A - LW - R\gamma g_{co_2}qWN^2.$$

J is the objective functional, $N_T(x)$ and $W_T(x)$ are the objective patterns and $N(x,t)$ and $W(x,t)$ are state variables. $r(x.t)$ is the control variable and b_1, b_2, c are the constant.

Next, we discuss the expression of an optimal solution.

Constructing Lagrange functional [41–45]:

$$
\begin{aligned}
L[N,W,r,v_1,v_2] =&J[N,W,r] + \int_0^T\int_\Omega[-\frac{\partial N}{\partial t} + D_N\triangle N + f_1(N,W,r)]v_1dxdt\\
&+\int_0^T\int_\Omega[-\frac{\partial W}{\partial t} + D_W\triangle W + f_2(N,W,r)]v_2dxdt\\
&+\int_0^T\int_{\partial\Omega}(-D_N\frac{\partial N}{\partial n})v_1dsdt + \int_0^T\int_{\partial\Omega}(-D_W\frac{\partial W}{\partial n})v_2dsdt\\
=&J[N,W] + \int_0^T\int_\Omega\frac{\partial v_1}{\partial t}Ndxdt + \int_\Omega[N(x,0)v_1(x,0) - N(x,T)v_1(x,T)]dx\\
&+\int_0^T\int_\Omega D_N\triangle v_1Ndxdt - \int_0^T\int_{\partial\Omega}\frac{\partial v_1}{\partial n}Ndsdt + \int_0^T\int_\Omega f_1(N,W,r)v_1dxdt\\
&+\int_0^T\int_\Omega\frac{\partial v_2}{\partial t}Wdxdt + \int_\Omega[W(x,0)v_2(x,0) - W(x,T)v_2(x,T)]dx\\
&+\int_0^T\int_\Omega D_W\triangle v_2Wdxdt - \int_0^T\int_{\partial\Omega}\frac{\partial v_2}{\partial n}Wdsdt + \int_0^T\int_\Omega f_2(N,W,r)v_2dxdt.
\end{aligned}
$$

Here, the local optimal solution of the optimal control problem is (N^*, W^*, r^*), for any small enough and smooth function $N(x,t)$ with $N(x,t) = 0$. By calculation, one has the directional derivative of the Lagrange functional at $(N^*, W^*, r^*, v_1, v_2)$, which satisfies the following equation:

$$
\begin{aligned}
0 =&L_N[N^*,W^*,r^*,v_1,v_2]\\
=&b_1\int_\Omega[N^*(x,T) - N_T(x)]N(x,T)dx\\
&+\int_0^T\int_\Omega\frac{\partial v_1}{\partial t}Ndxdt - \int_\Omega v_1(x,T)N(x,T)dx\\
&+\int_0^T\int_\Omega D_N\Delta v_1Ndxdt - \int_0^T\int_\Omega\frac{\partial v_1}{\partial n}Ndsdt + \int_0^T\int_\Omega f_{1,N}(N^*,W^*,r^*)v_1Ndxdt\\
&+\int_0^T\int_\Omega f_{2,N}(N^*,W^*,r^*)v_2Ndxdt.
\end{aligned}
$$

It follows from the arbitrariness of $N(x,t)$ that v_1 satisfies

$$
\begin{cases}
-\dfrac{\partial v_1}{\partial t} = D_N\Delta v_1 + f_{1,N}(N^*,W^*,r^*)v_1 + f_{2,N}(N^*,W^*,r^*)v_2,\\
\dfrac{\partial v_1}{\partial n} = 0,\\
v_1(x,T) = b_1[N^*(x,T) - N_T(x)].
\end{cases}
\tag{3.4}
$$

Analogously, one has

$$
\begin{aligned}
0 =& L_W[N^*, W^*, r^*, v_1, v_2] \\
=& b_2 \int_\Omega [W^*(x,T) - W_T(x)]W(x,T)dx \\
&+ \int_0^T \int_\Omega \frac{\partial v_2}{\partial t} W dxdt - \int_\Omega v_2(x,T)W(x,T)dx \\
&+ \int_0^T \int_\Omega D_W \Delta v_2 W dxdt - \int_0^T \int_\Omega \frac{\partial v_2}{\partial n} W dsdt + \int_0^T \int_\Omega f_{1,W}(N^*, W^*, r^*) v_1 W dxdt \\
&+ \int_0^T \int_\Omega f_{2,W}(N^*, W^*, r^*) v_2 W dxdt,
\end{aligned}
$$

and

$$
\begin{cases}
-\dfrac{\partial v_2}{\partial t} = D_W \Delta v_2 + f_{1,W}(N^*, W^*, r^*) v_1 + f_{2,W}(N^*, W^*, r^*) v_2, \\
\dfrac{\partial v_2}{\partial n} = 0, \\
v_2(x,T) = b_2[W^*(x,T) - W_T(x)].
\end{cases}
\tag{3.5}
$$

Substituting $f_{1,N}, f_{1,W}, f_{2,N}$ and $f_{2,W}$ into Eqs (3.4) and (3.5), the adjoint equation of (v_1, v_2) is:

$$
\begin{cases}
-\dfrac{\partial v_1}{\partial t} = D_N \Delta v_1 + 2W^* N^* R g_{co_2}(J v_1 - r v_2) - R_{esp} v_1, \\
-\dfrac{\partial v_2}{\partial t} = D_W \Delta v_2 + N^{*2} R g_{co_2}(J v_1 - r v_2) - L v_2, \\
\dfrac{\partial v_1}{\partial n} = 0, \\
\dfrac{\partial v_2}{\partial n} = 0, \\
v_1(x,T) = b_1[N^*(x,T) - N_T(x)], \\
v_2(x,T) = b_2[W^*(x,T) - W_T(x)].
\end{cases}
\tag{3.6}
$$

Note that the allowed control set is a closed convex set. It is clear that the directional derivative of the Lagrange functional at $(N^*, W^*, r^*, v_1, v_2)$ along $r - r^*$ satisfies:

$$
\begin{aligned}
0 \le& L_r[N^*, W^*, r^*, v_1, v_2] \\
=& c \int_0^T \int_\Omega r^*(r - r^*)dxdt + \int_0^T \int_\Omega f_{1,r}(N^*, W^*, r^*)(r - r^*) v_1 dxdt \\
&+ \int_0^T \int_\Omega f_{2,r}(N^*, W^*, r^*)(r - r^*) v_2 dxdt.
\end{aligned}
$$

Since r is arbitrary, we substitute $f_{1,r}$ and $f_{2,r}$ into the above inequality, then the following variational inequality can be obtained:

$$
\int_0^T \int_\Omega (c r^* + N^* v_1)(r - r^*)dxdt \ge 0. \tag{3.7}
$$

By the variational inequality (3.7), it follows that

$$r^* = P_{[r_1,r_2]}[-\frac{1}{c}N^* v_1],$$

where we define the projection P as

$$P_{[r_1,r_2]}(r) = max[r_1, min[r, r_2]].$$

4. The simulation results

4.1. Response of vegetation pattern to different climatic factors

In this section, we apply the biologically realistic parameters to perform the numerical simulations and research the response of vegetation pattern to climate change, which is based on the climatic data from 1969–2019 of Qinghai Lake. The average values of the climatic factors (precipitation, temperature and $[CO_2]$) are obtained and they are 1.05(mm/d), 0.9879(°C) and 396(ppm), respectively. The other parameters are fixed: $B_R = 1, Rh = 0.4, g_{co_2} = 10 * 10^{-3}, M_{10} = 1.6, R = 2.6 * 10^{-2}, \gamma = 2.5 * 10^3, C_1 = 12, \frac{C_i}{C_a} = 0.6, \rho = 0.24, D_N = 0.1, D_W = 100$.

Figures 2 and 3, respectively, show the effects of precipitation and $[CO_2]$ on vegetation pattern. We can observe that the vegetation patterns change from spot structure to stripe structure as increase of precipitation or $[CO_2]$. The highest density decreases gradually, the lowest density increases gradually and the distribution of vegetation is more uniform. Figure 4 illustrates the variation of vegetation patterns in regard to temperature. With increase of temperature, the transition of vegetation pattern experiences stripe and spot. In contrast with the first two meteorological factors, the highest density increases and the lowest density decreases and the distribution is more uneven, which is not conducive to the robustness of ecosystem. The three climatic factors have different effects on the mean density of vegetation. More precisely, the mean vegetation density is positively associated with rainfall and $[CO_2]$, which is in contrast to temperature. This is visualized in Figure 5.

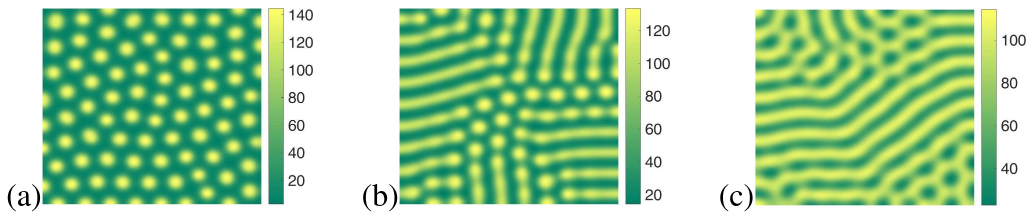

Figure 2. Evolution of vegetation pattern in regard to precipitation with parameters $[CO_2]$=396, T=0.9879. (a) A=0.8; (b) A=1.15; (c) A=1.4. As the increase of A, the robustness of the vegetation system is enhanced.

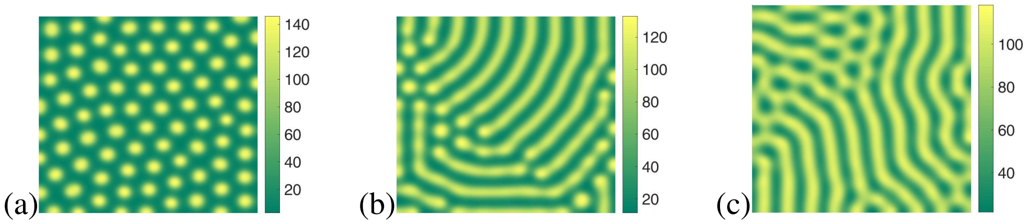

Figure 3. Evolution of vegetation pattern in regard to [CO_2] with parameters A=1.05, T=0.9879. (a) [CO_2]=370; (b) [CO_2]=400; (c) [CO_2]=440. The increase of [CO_2] improves the robustness of the vegetation system.

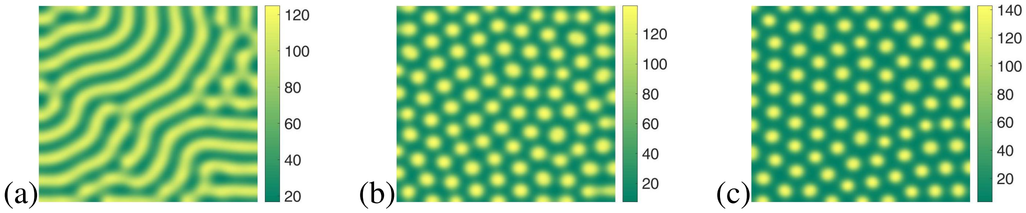

Figure 4. Evolution of vegetation pattern in regard to T with parameters A=1.05, [CO_2]=396. (a) T=0.9; (b) T=1.05; (c) T=1.2. The increase of T accelerates degradation of the vegetation system.

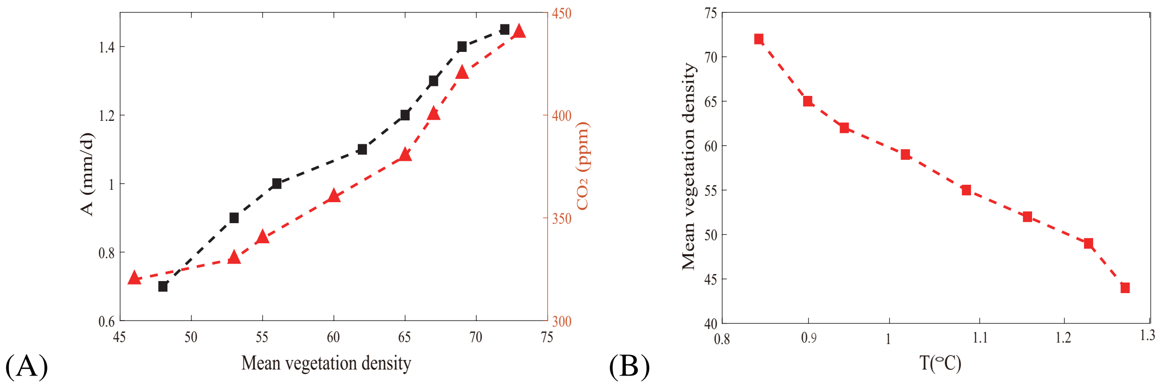

Figure 5. The effects of different climitic factors on mean vegetation density.

4.2. Prediction of vegetation pattern under different climate scenarios

In this section, we devote to forecast the future vegetation growth in Qinghai Lake area under three different climate scenarios. The three climate scenarios are simulated data selected from the Coupled Model Intercomparison Project Phase 5 (CMIP5) which has three representative concentration paths (RCP2.6, RCP4.5 and RCP8.5) [46–48]; see Table 1 for an introduction of CMIP5.

Table 1. The interpretation of different climate scenarios in CMIP5.

Scenario	Interpretation	$[CO_2]$ in 2100yr
RCP2.6	low radiative forcing scenario	440
RCP4.5	middle radiative forcing scenario	610
RCP8.5	high scenario with radiative forcing	1170

We adopt linear regression analysis to statistical temperature, $[CO_2]$ and rainfall data under three different scenarios to obtain climate change trends. The results are visualized in Table 2. Temperature and $[CO_2]$ increase under the three climate scenarios, and rainfall increases in RCP4.5 and RCP8.5. To predict the future evolution of vegetation pattern in regard to different climate scenarios, Figure 6 shows the variation of vegetation pattern. We can observe that vegetation pattern transitions with the increase of time in RCP2.6: Stripes → gap → uniform, which indicates that the robustness of the vegetation system is increasing. This is reasonable to infer that the increased robustness of the vegetation system is due to the increase of precipitation and $[CO_2]$. Compared with RCP2.6, the spatial distribution structure changes from stripe to spot in RCP4.5 and RCP8.5, which implies that the ecosystem may undergo degradation, which can finally lead to desertification.

Table 2. The change rate of three climitic factors in different scenarios.

Scenario	A(mm/d)	T(°C)	$[CO_2]$(ppm)
RCP2.6	0.002	0.0089	0.42
RCP4.5	-0.170	0.0273	2.10
RCP8.5	-0.471	0.0576	7.70

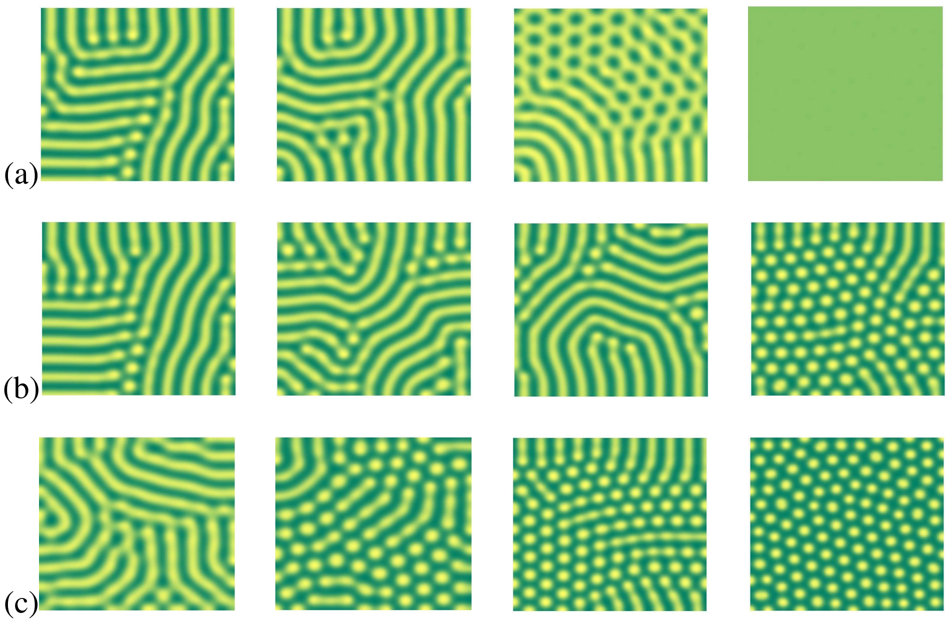

Figure 6. Evolution of vegetation pattern in regard to different times in different scenarios. (a) RCP2.6; (b) RCP4.5; (c) RCP8.5. From left to right, the corresponding time t (year) are t=2030, 2050, 2080 and 2100.

4.3. The optimal control

In order to increase the resilience of degraded ecosystem and avoid the occurrence of desertification, we offer the optimal conservation strategy−human activity (e.g. artificial planting). As illustrated in Figure 2, the transformation from stripe pattern to spot pattern occurs with decreasing precipitation, and spot structure can serve as an early warning signal of the catastrophic shift [49]. Moreover, the precipitation has a significant impact on the spatial distribution structure of vegetation. Choose a pattern structure corresponding to $A = 1.3$ as the target pattern, which represents a robust ecological structure. In Figure 7, the snapshots of the optimal control $r(x, t)$ and the associated state variable $N(x, t)$ at rainfall $A = 0.8$ and 1.15 are presented, respectively. Consequently, artificial planting is an effective way to transform the vegetation pattern into an ideal state.

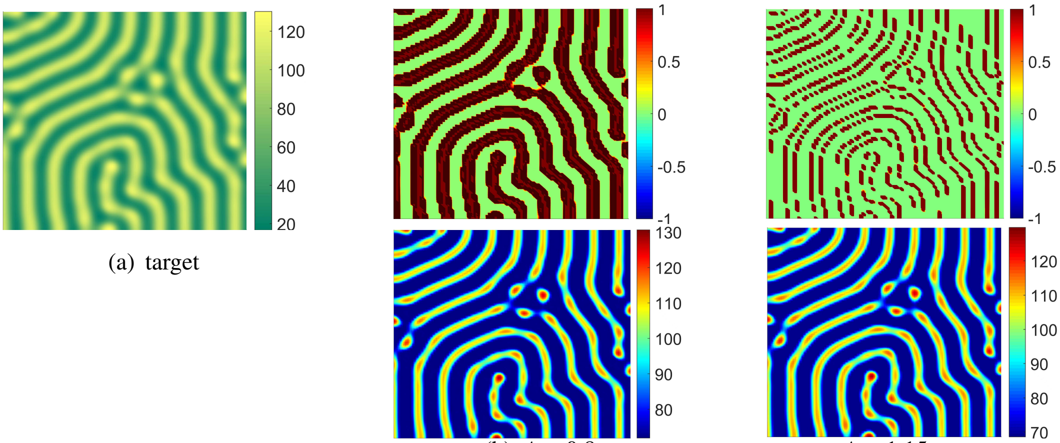

(a) target (b) $A = 0.8$ $A = 1.15$

Figure 7. (a) The target pattern when $A = 1.3$. (b) The optimal control r (top) and the controlled solution N (bottom) when $A = 0.8$ and $A = 1.15$, respectively.

5. Conclusions and discussion

For the last few decades, global climate has been facing a great change. The vegetation system exhibits a sensitive response to climate change, especially in arid and semi-arid regions. In this paper, we chose Qinghai Lake as the study area, which is a typical semi-arid area, and studied the response of vegetaion pattern to climate change. We developed a vegetation-water system (2.4) with climatic factors by the zero-flux Neumann conditions and investigated the dynamical behavior. First, we showd the stability of the constant equilibria for (2.4) without diffusion. Moreover, we analyzed the spatiotemporal dynamics at the constant equilibria with diffusion. The conditions for Turing instability of the positive constant equilibrium were obtained in the framework of Turing principle.

Our findings in numerical results revealed that the variation of data for climatic factors had a major impact on vegetation pattern. As precipitation or $[CO_2]$ increased, the robustness of the vegetation system was enhanced and the mean density increased. Unlike the first two climatic factors, rising temperatures not only lead to the emergence of spot pattern, but also reduced the mean density of vegetation and accelerated the degradation of the vegetation system. Furthermore, in order to forecast the future vegetation growth in Qinghai Lake, we presented evolution of the vegetation system under different climate scenarios. The results showed that the vegetation system collapses to desertification state in the future in RCP4.5 and RCP8.5 scenarios. This results from the synergy of precipitation, temperature and [CO_2]. Compared to RCP4.5 and RCP8.5, due to the dual effects of the increase of precipitation and [CO_2], RCP2.6 is a desired climate scenario for Qinghai Lake.

A direction for further study is how to timely avoid desertification. Owing to the method of optimal control, we can induce phase transitions between different vegetation pattern through human activities, such as artificial planting. More precisely, any presented pattern structure (e.g. spot pattern, strip pattern, and gap pattern) can be transformed into a desired pattern (see the Figure 7). As a result, artificial planting contributes to guarding against desertification of vegetation systems, even in low-rainfall regions. The result certifies the effectiveness of the optimal-control method in respect of prevention and control desertification.

This study highlighted the response of vegetation to climate change (precipitation, temperature and [CO_2] from modeling point of view. It is necessary to take other climatic factors into account, for instance, light, evaporation and humidity. Based on the seasonality of climate change, another aspect for future work would be to consider the nonautonomous systems; that is, all climatic factors considered in the model are coupled as a function of time. Furthermore, previous work has revealed that spot structure can provide early warning signal for catastrophic shift [49], which is from a qualitative point of view. From the quantitative perspectives, we expect to propose a quantifiable indicator for desertification evaluation, and this is also one of the key points for future research.

Use of AI tools declaration

The authors declare they have not used Artificial Intelligence (AI) tools in the creation of this article.

Acknowledgments

Fundamental Research Program of Shanxi Province (Grant Nos. 202203021212327 and 202203021211213), Program for the (Reserved) Discipline Leaders of Taiyuan Institute of Technology, Taiyuan Institute of Technology Scientific Research Initial Funding.

Conflict of Interest

The authors declare no conflict of interest.

References

1. Z. Wu, N. E. Huang, J. M. Wallace, B. V. Smoliak, X. Chen, On the time-varying trend in global-mean surface temperature, *Clim. Dynam.*, **37** (2011), 759–773. https://doi.org/10.1007/s00382-011-1128-8
2. J. Huang, X. Guan, F. Ji, Enhanced cold-season warming in semi-arid regions, *Atmos. Chem. Phys.*, **12** (2012), 5391–5398. https://doi.org/10.5194/acp-12-5391-2012
3. A. Dai, Drought under global warming: A review, *WIREs. Clim. Change*, **2** (2011), 45–65. https://doi.org/10.1002/wcc.81

4. J. Hansen, R. Ruedy, M. Sato, K. Lo, Global surface temperature change, *Rev. Geophys.*, **48** (2010). https://doi.org/10.1029/2010RG000345
5. Z. Li, J. Gao, L. Wen, C. Zou, C. Feng, D. Li, et al., Dynamics of soil respiration in alpine wetland meadows exposed to different levels of degradation in the Qinghai-Tibet Plateau, China, *Sci. Rep.*, **9** (2019), 7469. https://doi.org/10.1038/s41598-019-43904-1
6. J. Gao, H. Ouyang, G. Lei, X. Xu, M. Zhang, Effects of temperature, soil moisture, soil type and their interactions on soil carbon mineralization in Zoigo alpine wetland, Qinghai-Tibet Plateau, *Chinese Geogr. Sci.*, **21** (2011), 27–35. https://doi.org/10.1007/s11769-011-0439-3
7. C. Mu, T. Zhang, Q. Zhao, H. Su, S. Wang, B. Cao, et al., Permafrost affects carbon exchange and its response to experimental warming on the northern Qinghai-Tibetan Plateau, *Agr. Forest Meteorol.*, **247** (2017), 252–259. https://doi.org/10.1016/j.agrformet.2017.08.009
8. F. Peng, Q. G. You, M. H. Xu, X. H. Zhou, T. Wang, G. Guo, et al., Effects of experimental warming on soil respiration and its components in an alpine meadow in the permafrost region of the Qinghai-Tibet Plateau, *Eur. J. Soil Sci.*, **66** (2015), 145–154. https://doi.org/10.1111/ejss.12187
9. Z. X. Xu, T. L. Gong, J. Y. Li, Decadal trend of climate in the Tibetan Plateaui-regional temperature and precipitation, *Hydrol. Process.*, **22** (2008), 3056–3065. https://doi.org/10.1002/hyp.6892
10. G. Zhang, T. Yao, H. Xie, K. Yang, L. Zhu, C. K. Shum, et al., Response of Tibetan Plateau lakes to climate change: Trends, patterns, and mechanisms, *Earth Sci. Rev.*, **208** (2020), 103269. https://doi.org/10.1016/j.earscirev.2020.103269
11. J. Wang, Q. Wu, Impact of experimental warming on soil temperature and moisture of the shallow active layer of wet meadows on the Qinghai-Tibet Plateau, *Cold Reg. Sci. Technol.*, **90-91** (2013), 1–8. https://doi.org/10.1016/j.coldregions.2013.03.005
12. W. Wan, L. Zhao, H. Xie, B. Liu, H. Li, Y. Cui, et al., Lake surface water temperature change over the Tibetan plateau from 2001 to 2015: A sensitive indicator of the warming climate, *Geophys. Res. Lett.*, **45** (2018), 11177–11186. https://doi.org/10.1029/2018GL078601
13. G. Wang, Y. Li, Q. Wu, Y. Wang, Impacts of permafrost changes on alpine ecosystem in Qinghai-Tibet Plateau, *Sci. China Ser. D*, **49** (2006), 1156–1169. https://doi.org/10.1007/s11430-006-1156-0
14. X. Wu, L. Zhao, M. Chen, H. Fang, G. Yue, J. Chen, et al., Soil organic carbon and its relationship to vegetation communities and soil properties in permafrost areas of the Central Western Qinghai-Tibet Plateau, China, *Permafrost Periglac. Process.*, **23** (2012), 162–169. https://doi.org/10.1002/ppp.1740
15. X. Wu, H. Fang, Y. Zhao, J. M. Smoak, W. Li, W. Shi, et al., A conceptual model of the controlling factors of soil organic carbon and nitrogen densities in a permafrost-affected region on the eastern Qinghai-Tibetan Plateau, *J. Geophys. Rese. Biogeo.*, **122** (2017), 1705–1717. https://doi.org/10.1002/2016JG003641
16. S. Cao, G. Cao, Q. Feng, G. Han, Y. Lin, J. Yuan, et al., Alpine wetland ecosystem carbon sink and its controls at the Qinghai Lake, *Environ. Earth Sci.* **76** (2017), 210. https://doi.org/10.1007/s12665-017-6529-5

17. X. Li, W. Liu, L. Xu, Carbon isotopes in surface-sediment carbonates of modern Lake Qinghai (Qinghai-Tibet Plateau): Implications for lake evolution in arid areas, *Chem. Geol.*, **300** (2012), 88–96. https://doi.org/10.1016/j.chemgeo.2012.01.010

18. H. Ao, C. Wu, X. Xiong, L. Jing, X. Huang, K. Zhang, et al., Water and sediment quality in Qinghai Lake, China: A revisit after half a century, *Environ. Monit. Assess.*, **186** (2014), 2121–2133. https://doi.org/10.1007/s10661-013-3522-7

19. L. Tang, X. Duan, F. Kong, F. Zhang, Y. Zheng, Z. Li, et al., Influences of climate change on area variation of Qinghai Lake on Qinghai-Tibetan Plateau since 1980s, *Sci. Rep.*, **8** (2018), 7331. https://doi.org/10.1038/s41598-018-25683-3

20. B. Chang, K. N. He, R. J. Li, Z. P. Sheng, H. Wang, Linkage of climatic factors and human activities with water level fluctuations in Qinghai Lake in the northeastern Tibetan Plateau, China, *Water*, **9** (2017), 552. https://doi.org/10.3390/w9070552

21. C. Fan, C. Song, W. Li, K. Liu, J. Cheng, C. Fu, et al., What drives the rapid water-level recovery of the largest lake (Qinghai Lake) of China over the past half century?, *J. Hydrol.*, **593** (2021), 125921. https://doi.org/10.1016/j.jhydrol.2020.125921

22. H. Dong, Y. Song, M. Zhang, Hydrological trend of Qinghai Lake over the last 60 years: Driven by climate variations or human activities? *J. Water Climate Change*, **10** (2019), 524–534. https://doi.org/10.2166/wcc.2018.033

23. W. Zhang, S. Wang, B. Zhang, F. Zhang, Q. Shen, Y. Wu, et al., Analysis of the water color transitional change in Qinghai Lake during the past 35 years observed from Landsat and MODIS, *J. Hydrol. Reg. Stud.*, **42** (2022), 101154. https://doi.org/10.1016/j.ejrh.2022.101154

24. T. Che, X. Li, R. Jin, Monitoring the frozen duration of Qinghai Lake using satellite passive microwave remote sensing low frequency data, *Chin. Sci. Bull.*, **54** (2009), 2294–2299. https://doi.org/10.1007/s11434-009-0044-3

25. L. Feng, J. Liu, T. A. Ali, J. S. Li, J. Li, S. Kuang, Impacts of the decreased freeze-up period on primary production in Qinghai Lake, *Int. J. Appl. Earth Obs.*, **83** (2019), 101915. https://doi.org/10.1016/j.jag.2019.101915

26. Z. Jin, C. F. You, Y. Wang, Y. Shi, Hydrological and solute budgets of Lake Qinghai, the largest lake on the Tibetan Plateau, *Quatern. Int.*, **218** (2010), 151–156. https://doi.org/10.1016/j.quaint.2009.11.024

27. N. Zhang, X. Cao, Q. Xu, X. Huang, U. Herzschuh, Z. Shen, et al., Vegetation change and human-environment interactions in the Qinghai Lake Basin, northeastern Tibetan Plateau, since the last deglaciation, *CATENA*, **210** (2022), 105892. https://doi.org/10.1016/j.catena.2021.105892

28. X. Wang, T. Liang, H Xie, X. Huang, H. Lin, Climate-driven changes in grassland vegetation, snow cover, and lake water of the Qinghai Lake basin, *J. Appl. Remote Sens.*, **10** (2016), 036017. https://doi.org/10.1117/1.JRS.10.036017

29. H. Zhang, L. Tian, E. Hasi, D. Zhang, W. Wu, Vegetation-soil dynamics in an alpine desert ecosystem of the Qinghai Lake watershed, northeastern Qinghai-Tibet Plateau, *Front. Environ. Sci.*, **11** (2023), 1119605. https://doi.org/10.3389/fenvs.2023.1119605

30. Y. Cai, J. Zhang, N. Yang, C. Zhang, C. Zhao, H. Long, Human impacts on vegetation exceeded the hydroclimate control 2 ka ago in the Qinghai Lake basin revealed by n-alkanes of loess, *Palaeogeogr. Palaeocl.*, **607** (2022), 111269. https://doi.org/10.1016/j.palaeo.2022.111269

31. Z. Chen, J. Liu, L. Li, Y. P. Wu, G. Feng, Z. Qian, et al., Effects of climate change on vegetation patterns in Hulun Buir Grassland, *Phys. A*, **597** (2022), 127275. https://doi.org/10.1016/j.physa.2022.127275

32. G. Q. Sun, C. H. Wang, L. L. Chang, Y. P. Wu, L. Li, Z. Jin, Effects of feedback regulation on vegetation patterns in semi-arid environments, *Appl. Math. Model.*, **61** (2018), 200–215. https://doi.org/10.1016/j.apm.2018.04.010

33. J. Liang, C. liu, G. Q. Sun, L. li, L. Zhang, M. Hou, et al., Nonlocal interactions between vegetation induce spatial patterning, *Appl. Math. Comput.*, **428** (2022), 127061. https://doi.org/10.1016/j.amc.2022.127061

34. Q. Xue, G. Q. Sun, C. Liu, Z. G. Guo, Z. Jin, Y. P. Wu, et al., Spatiotemporal dynamics of a vegetation model with nonlocal delay in semi-arid environment, *Nonlinear Dyn.*, **99** (2020), 3407–3420. https://doi.org/10.1007/s11071-020-05486-w

35. M. R. Aguiar, O. E. Sala, M. R. Aguiar, O. E. Sala, Patch structure, dynamics and implications for the functioning of arid ecosystems, *Trends Ecol. Evol.*, **14** (1999), 273–277. https://doi.org/10.1016/S0169-5347(99)01612-2

36. C. A. Klausmeier, Regular and irregular patterns in semiarid vegetation, *Science*, **284** (1999), 1826–1828. https://doi.org/10.1126/science.284.5421.1826

37. S. Kéfi, M. Rietkerk, G. G. Katul, Vegetation pattern shift as a result of rising atmospheric CO_2 in arid ecosystems, *Theor. Popul. Biol.*, **74** (2008), 332–344. https://doi.org/10.1016/j.tpb.2008.09.004

38. X. Tang, Y. Song, T. Zhang, Turing-Hopf bifurcation analysis of a predator-prey model with herd behavior and cross-diffusion, *Nonlinear Dyn.*, **86** (2016), 73–89. https://doi.org/10.1007/s11071-016-2873-3

39. W. Zuo, Y. Song, Stability and bifurcation analysis of a reaction-diffusion equation with distributed delay, *Nonlinear Dyn.*, **79** (2015), 437–454. https://doi.org/10.1007/s11071-014-1677-6

40. M. R. Garvie, C. Trenchea, Optimal control of a nutrient-phytoplankton-zooplankton-fish system, *SIAM J. Control Optim.*, **46** (2007), 775–791. https://doi.org/10.1137/050645415

41. S. Lee, G. Chowell, Exploring optimal control strategies in seasonally varying flu-like epidemics, *J. Theor. Biol.*, **412** (2017), 36–47. https://doi.org/10.1016/j.jtbi.2016.09.023

42. L. Chang, S. Gao, Z. Wang, Optimal control of pattern formations for an SIR reaction-diffusion epidemic model, *J. Theor. Biol.*, **536** (2022), 111003. https://doi.org/10.1016/j.jtbi.2022.111003

43. L. Chang, W. Gong, Z. Jin, G. Q. Sun, Sparse optimal control of pattern formations for an SIR reaction-diffusion epidemic model, *SIAM J. Appl. Math.*, **82** (2022), 1764–1790. https://doi.org/10.1137/22M1472127

44. W. Choi, E. Shim, Optimal strategies for social distancing and testing to control COVID-19, *J. Theor. Biol.*, **512** (2021), 110568. https://doi.org/10.1016/j.jtbi.2020.110568

45. S. Kim, J. Lee, E. Jung, Mathematical model of transmission dynamics and optimal control strategies for 2009 A/H1N1 influenza in the Republic of Korea, *J. Theor. Biol.*, **412** (2017), 74–85. https://doi.org/10.1016/j.jtbi.2016.09.025

46. K. E. Taylor, R. J. Stouffer, G. A. Meehl, An overview of CMIP5 and the experiment design, *Bull. Amer. Meteorol. Soc.*, **93** (2012), 485–498. https://doi.org/10.1175/BAMS-D-11-00094.1

47. K. Calvin, B. Bond-Lamberty, L. Clarke, J. Edmonds, J. Eom, C. Hartin, et al., The SSP4: A world of deepening inequality, *Global Environ. Chang*, **42** (2017), 284–296. https://doi.org/10.1016/j.gloenvcha.2016.06.010

48. T. Zhao, L. Chen, Z. Ma, Simulation of historical and projected climate change in arid and semiarid areas by CMIP5 models, *Chin. Sci. Bull.*, **59** (2014), 412–429. https://doi.org/10.1007/s11434-013-0003-x

49. J. von Hardenberg, E. Meron, M. Shachak, Y. Zarmi, Diversity of vegetation patterns and desertification, *Phys. Rev. Lett.*, **87** (2001), 198101. https://doi.org/10.1103/PhysRevLett.87.198101

Appendix A. Model notation and interpretation

Parameter	Interpretation	Unit
g_{co_2}	Maximal leaf conductance to CO_2	$mod\ m^{-2}d^{-1}$
γ	Conversion coefficient from maximal leaf conductance to water vapor to maximal leaf conductance CO_2	$mm\ m^{-2}mol^{-1}$
C_a	Ambient CO_2 concentration	$mol\ mol^{-1}$
C_i	Intercellular CO_2 concentration	$mol\ mol^{-1}$
C_1	Coefficient of conversion of photosynthesis (mol) into biomass (g)	$g\ mol^{-1}$
B_R	Respiration per unit of biomass	d^{-1}
$s^*(T)$	Saturated vapor pressure	kPa
$s(T)$	Vapor pressure at T	kPa
R_h	Relative humidity $\frac{e(T)}{e^*(T)}$	-
R	The water uptake by roots	mm/d
P	The ground pressure	kPa
ρ	Reduced evaporation rate of vegetation due to shading	-
T	Temperature	$^{\circ}C$
A	Rainfall	$(mmd)^{-1}$
t	time	d